Sensors & Actuators: B. Chemical 445 (2025) 138604

Contents lists available at ScienceDirect

Sensors and Actuators: B. Chemical

journal homepage: www.elsevier.com/locate/snb

Multiplex on-chip immunosensor for advancing inflammation biomarkers monitoring

Nadia Moukri [a,*], Vuslat Juska [b,*], Bernardo Patella [a], Maria Rita Giuffrè [c], Elisabetta Pace [d], Chiara Cipollina [c], Alan O'Riordan [b], Rosalinda Inguanta [a]

[a] Department of Engineering, University of Palermo, Palermo 90128, Italy
[b] Precision Electrochemical Nanosensor Group, Tyndall National Institute, University College Cork, Cork T12 R5CP, Ireland
[c] Ri.MED Foundation, Palermo 90146, Italy
[d] Institute of Translational Pharmacology (IFT), National Research Council of Italy (CNR), Palermo 90146, Italy

ARTICLE INFO

Keywords:
Multiplex immunosensor
Biomarkers
Gold foam
Interleukin 8
Immunoglobulin G
Macrophages

ABSTRACT

Chronic inflammatory diseases significantly impact quality of life and healthcare resources. Continuous monitoring of biomarkers in easily accessible biological fluids presents a promising strategy to enhance management, optimize treatments, and improve patient outcomes. Interleukin-8 (IL-8) is a pro-inflammatory cytokine whose levels increase during chronic airways inflammatory diseases and can be found in human saliva. To this end, electrochemical immunosensors which can effectively detect clinically relevant biomarkers, while also offering the benefits of miniaturization and portability will enable telemedicine applications for remote monitoring and personalized healthcare. In this work, we developed an advanced electrochemical multiplex immunosensor platform using gold micro-electrodes modified by the electrochemical deposition of a gold foam and an anti-fouling polymeric layer. The sensor capability for multiple detection was evaluated by measuring human interleukin 8 (H-IL8) and human immunoglobulin G (H-IgG) (the latter used as a model analyte). Immunosensors exhibited high sensitivity even in complex biological samples such as human serum and artificial saliva. A very low detection limit of 69.2 fg mL^{-1} for H-IgG and 87.6 fg mL^{-1} for H-IL8 in phosphate buffered saline was established. To assess real-world applicability, the immunosensor was used to quantify H-IL8 release from primary human monocyte-derived macrophages stimulated with pro-inflammatory bacterial lipopolysaccharide and the results were successfully compared with ELISA. Furthermore, the sensor performance was also demonstrated in real biological fluids by detecting H-IL8 in spiked human saliva.

1. Introduction

In recent years, there has been a growing demand for on-site, rapid, and accurate testing devices for biomarker monitoring within the biomedical sector [1]. The use of these devices can be particularly helpful in managing chronic inflammatory diseases, which present significant challenges due to the necessity for continuous analysis in the absence of definitive cures [2]. Airway-associated conditions like asthma and chronic obstructive pulmonary disease (COPD) affect millions of people globally, making their monitoring and treatment crucial for most healthcare systems [3,4]. Their chronic nature leads to considerable negative impacts on quality of life and resource utilization, such as the need for frequent healthcare visits, hospitalizations, and the ongoing requirement for long-term therapy [5]. Inflammatory conditions are associated with the increase (both local and systemic) of inflammatory mediators [6]. Cytokines (such as lymphokines, interleukins, and chemokines) are small proteins (less than 40 kDa) released by cells that play a key role in the inflammatory process [7].

List of acronyms: Anti-H-IgG, Human Immunoglobulin G Antibody; Anti-H-IL8, Human Interleukin-8 Antibody; BSA, Bovine Serum Albumin; CLSM, Confocal Laser Scanning Microscopy; COPD, Obstructive Pulmonary Disease; Cs, Chitosan; CV, Cyclic Voltammetry; DPV, Differential Pulse Voltammetry; ELISA, Enzyme-Linked Immunosorbent Assay; Fab, The Antigen-Binding Region; Fc, Fragment Crystallizable; FBS, Fetal Bovine Serum; GO, Graphene Oxide; H-IgG, Human Immunoglobulin G; H-IL8, Human Interleukin-8; HMDMs, Human Monocyte-Derived Macrophages; LOD, Limit of Detection; LPS, Lipopolysaccharide; MEA, Multi-Electrode Array; PBS, Phosphate-Buffered Saline; PBMCs, Peripheral Blood Mononuclear Cells; RGO, Reduced Graphene Oxide; WE, Working Electrode.

* Corresponding authors.
E-mail addresses: nadia.moukri@unipa.it (N. Moukri), vuslat.juska@tyndall.ie (V. Juska).

https://doi.org/10.1016/j.snb.2025.138604
Received 28 May 2025; Received in revised form 14 August 2025; Accepted 25 August 2025
Available online 27 August 2025

Their increase in biological fluids is often linked to disease onset, progression, or reacutization. Furthermore, with the recent emergence of new biologic therapies based on monoclonal antibodies targeting specific cytokines [8], monitoring cytokines has become essential for ensuring the optimal selection of patients and assessing treatment efficacy. For these reasons, continuous monitoring of cytokines in easily accessible biological fluids would greatly enhance overall disease management. Among cytokines, Interleukin-8 (H-IL8) is of particular interest as it is linked with several inflammatory diseases, including asthma and COPD [9].

Electrochemical immunosensors that exploit the specificity of antibody recognition [10] are highly effective tools for developing advanced devices for detecting clinically relevant biomarkers [11]. The complexity of inflammatory diseases necessitates simultaneous analysis of different biomarkers to achieve a more comprehensive and robust understanding of disease status [12]. Multi-analyte detection can be performed using devices with a single electrode [13] or a multi-electrode array (MEA) [14]. For MEA, photolithography microfabrication is a suitable technique for obtaining several electrodes on the same miniaturized platform, including reference and counter electrodes [15].

Cytokines can be found in biological fluids at extremely low concentrations [16,17]. As an example, serum IL-8 levels are in the low pg/mL range in COPD and asthma patients [18,19] while concentration of IL-8 in saliva can reach the low ng/mL range in asthma patients [20]. A key aspect when developing approaches for non-invasive biomarker monitoring is the selection of the right biological fluid, which should be easy to collect and directly related to the disease-relevant body compartment. In the case of cytokine detection for airway inflammation, saliva fulfils these requirements [21]. Numerous studies have demonstrated a significant increase in IL-8 levels in the saliva of patients with asthma [22,23]. The research challenge is to develop highly sensitive, selective sensors with a low limit of detection (LOD). These goals can be achieved using different strategies that involve the substrate, antibody immobilization, and antifouling layers. For substrates, nanomaterials [24] are particularly beneficial as they enhance immunosensor performance by improving biomolecule immobilization [25] and amplifying the electrochemical signal due to a higher surface area [26].

A crucial step in immunosensor development is antibody immobilization on the electrode surface. Affinity immobilization is among the most efficient techniques [27] for achieving stable and oriented binding. The widely used affinity immobilization relies on ligand mediators like protein A or G [28] which exhibit strong biological affinity for the fragment crystallizable (Fc) region of antibodies. This approach ensures that the Fc region binds to the electrode surface without involving the antigen-binding (Fab) region. To increase the selectivity of immunosensors toward the analyte of interest (an essential characteristic for immunosensors operating in highly complex biological fluids, such as serum, blood, saliva, etc. [29]), it is critical to avoid non-specific adsorption of coexisting species (proteins, peptides, lipids, and hormones) [30]. To improve this aspect, electrodes can be functionalized with anti-fouling materials, including hydrogels such as chitosan [31] or protein like bovine serum albumin (BSA) [32].

In this work, we developed an electrochemical multiplex immunosensor platform using microdisk electrodes modified with nanostructured gold foam and an antifouling polymeric layer. The substrate was a lithographically fabricated device with three-disc gold working micro-electrodes. Each electrode was first modified with gold foam obtained via hydrogen bubble template electrochemical deposition. An antifouling layer was then deposited on the gold foam by co-electrodeposition of chitosan (Cs), graphene oxide (GO), and BSA (Cs/rGO/BSA). The Cs/rGO/BSA layer also provided functionalities to covalently anchor Protein A/G on the electrode for achieving site-oriented antibody immobilization. The multiplexed detection capability of the sensors was examined for H-IL8 and human immunoglobulin G (H-IgG). H-IgG was chosen as a model analyte because it is the most prevalent isotype antibody in the bloodstream, making it ideal for optimizing all manufacturing parameters and assessing multiple detections alongside H-IL8. The developed immunosensor exhibited high sensitivity and low LOD for both target analytes in phosphate-buffered saline (PBS) and even in complex matrices such as human serum and artificial saliva. To evaluate its applicability for in vitro research studies, the sensor was employed to measure the concentration of H–IL8 released by primary human monocyte-derived macrophages (hMDMs) stimulated with the pro-inflammatory bacterial lipopolysaccharide (LPS). The sensor performance was also assessed in real human fluids by measuring the concentration of H-IL8 in spiked saliva samples.

2. Materials and methods

2.1. Materials and microchip fabrication

Chitosan, Bovine Serum Albumin (BSA), acetic acid, potassium chloride (KCl), sodium chloride (NaCl), potassium ferrocyanide ($K_4[Fe(CN)_6]$), potassium ferricyanide ($K_3[Fe(CN)_6]$), acetone, sterile human serum, PBS tablets (0.01 M, pH7.4), gold(III)chloride trihydrate, sulphuric acid, glutaraldehyde, H-IgG polyclonal antibody, H-IgG, Human IL8, were purchased from Sigma-Aldrich. Protein A/G, IgG binding buffer, Superblock buffer, IL8 polyclonal antibody, anti-Mouse IgG (Alexa Fluor Plus 405) were purchased from Thermo Fisher Scientific. Graphene oxide water dispersion was obtained from Graphenea.

The microchip pattern consisted of two rectangular gold electrodes serving as the counter and reference electrodes, and three gold working electrodes with a diameter of 100 μm. Device fabrication is detailed in previous work [15]. The substrate is a silicon wafer on which the device pattern was created by metal photolithography (Fig. 1-a). The obtained microchip had a compact design with an overall surface area of 45 mm^2. Due to the small size, 111 chips can be obtained from a 100 mm diameter silicon wafer (Fig. 1-a,b). Before use each chip was cleaned at least three times, alternating between acetone and water rinses.

Each gold working electrode (WE) on the chip was first modified with gold foam. Hydrogen bubble templated electrochemical deposition was carried out by applying staircase voltammetry from 0 to − 4 V vs Ag/AgCl, with a scan rate of 90 mV s^{-1} and a step height of 8.4 mV. A 2.8 M H_2SO_4 aqueous solution containing of 6 mM $HAuCl_4{\cdot}3H_2O$ was used as the deposition bath.

For the antifouling layer electrodeposition, stock solutions of chitosan and thermally denatured BSA were prepared. For chitosan solution, 20 mL of 0.1 M acetic acid containing 0.1 g of chitosan, was used. The solution of BSA (5 % wt) was denatured in a thermocycler (SimpliAmp™ Thermal Cycler, Thermo Fisher Scientific) at 50 °C for 5 min and 70 °C for 2 min (5 cycles). The antifouling deposition bath was prepared by diluting 50 μL of GO solution (4 mg mL^{-1}), 100 μL of denatured BSA solution, and 200 μL of chitosan solution in 6.3 mL water. The Cs/rGO/BSA co-deposition was performed via staircase voltammetry from 0 to − 1.1 V vs Ag/AgCl, with a scan rate of 7.5 mV s^{-1} and a step height of 2.5 mV. Gold foam and Cs/rGO/BSA depositions were performed with an external platinum wire and Ag/AgCl as counter and reference electrodes, respectively. After the depositions, electrodes were cleaned using deionized water and 0.2 M PBS (pH 7), and dried under a flow of nitrogen at room temperature.

2.2. Immunosensor assembling

The immunosensor assembly consisted of different steps. First, 5 μL of 1.5 % glutaraldehyde water solution was drop-cast on a working electrode. Then, the chips were incubated overnight at 4 °C in a vapor chamber to prevent droplet evaporation. The chips were then dried and 5 μL of a solution of Protein A/G 0.2 μg mL^{-1} (prepared using PBS 25 mM, pH 7) was drop-cast onto the pre-prepared working electrode surfaces. The chips were then incubated in a vapor chamber for 2 h at room temperature. The unbound surface was then blocked with 5 μL of

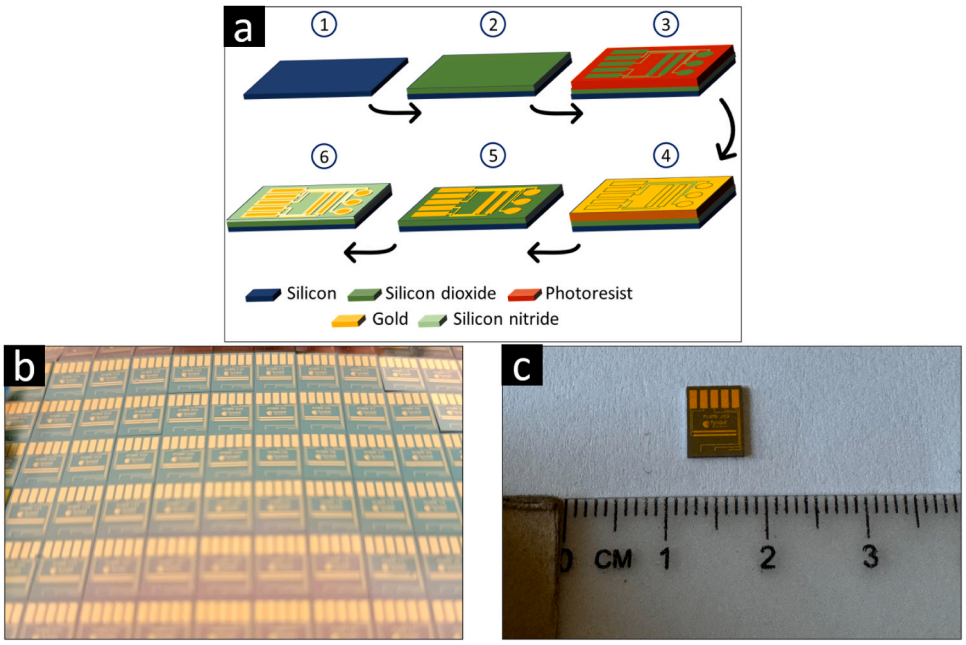

Fig. 1. a) Microfabrication scheme (1) Silicon wafer; (2) Silicon dioxide growth; (3) Photoresist mask; (4) Gold deposition; (5) Lift off; (6) Passivation layer and etching; b) Micro-chip silicon wafer image; c) micro-chip picture.

Superblock® in a vapor chamber for 20 min.

Anti-H-IgG (human immunoglobulin G antibody) or anti-H-IL8 (human Interleukin-8 antibody) was then immobilized onto the protein A/G modified electrodes. To optimize the antibody concentration, different dilutions in IgG binding buffer® were tested, ranging from 1 to 20 μg mL^{-1}. A 0.5 μL droplet was drop-cast onto a working electrode and incubated for 75 min at room temperature in a vapor chamber.

Sensors were calibrated for both target molecules, H-IgG and H-IL8, in PBS, human serum, and artificial saliva. In all cases, the investigated concentration range was from 1 fg mL^{-1} to 100 pg mL^{-1}. 5 μL of target solution was drop-cast on a working electrode and incubated for 30 min at room temperature. Blank negative controls were obtained by incubating the sensor (30 min) using PBS, artificial saliva, and human serum without the target protein.

After each incubation step, chips were washed gently with PBS (25 mM) to remove any unbound reagent excess and dried at room temperature. Incubations were carried out using an orbital shaker (Digital Microplate Shaker, Thermo Fisher Scientific) at 100 rpm.

2.3. Electrochemical and physical-chemical characterizations

For the electrochemical characterization, a redox probe solution containing $Fe(CN)_6^{3-/4-}$ 5 mM and KCl 1 M, was prepared in PBS. Cyclic voltammetry (CV) was performed from − 0.25 to 0.25 V vs Au, with a scan rate ranging from 10 to 300 mV s^{-1}. Differential pulse voltammetry (DPV) was employed as the detection technique in the potential range from − 0.3 to 0.2 V vs Au. DPV was performed (optimized parameters: 5 mV potential step, 50 ms modulation time, 100 ms interval time) before and after incubation with the target analyte. Using the redox probe solution, the sensor response (evaluated measuring ΔI, that is the difference between the current measured before (I_o) and after target incubation (I)) was assessed throughout the variation of the $Fe(CN)_6^{3-/4-}$ oxidation peak current. For this characterization, a 10 μL droplet of probe solution was deposited on the chip, covering the three working electrodes as well as the internal gold counter and reference electrodes. An Autolab (PGSTAT302N) Metrohm potentiostat was used for all the electrochemical tests and the Nova 2.1.5 software to process and analyze the signals.

A Carl Zeiss Supra 40 Scanning Electron Microscope (SEM), was used for morphological analysis. Confocal Laser Scanning Microscopy with excitation by a 647 nm Multiline Argon Laser (CLSM) was carried out using a FluoView 1000 (Olympus) equipped with 60X (PLAPON, NA1.35) and 100X (UPLSAPO, NA1.4) oil immersion objectives. The microscope was equipped with three filter cubes mounted on the scope: DAPI/Hoechst (ex 360–370, em 420–500), FITC/EGFP/Bodipy/Fluo3/Di O (ex 470–490, em 515–555) and TRITC, Rhodamine, Di I (ex 530–550, em 590–640). Energy-dispersive X-ray (EDS) and Raman spectroscopy were carried out to evaluate the change in compositions of the WEs after the different deposition steps used to prepare the immunosensor substrate. The Raman spectra were obtained using a Renishaw (inVia Raman Microscope) spectrometer. The excitation was provided by the 532 nm line of a Nd:YAG laser calibrated by the Raman peak of polycrystalline Si (520 cm^{-1}). FTIR characterization was carried out using a IRTracer-100 (SHIMADZU).

2.4. Culturing of human monocyte-derived macrophages (hMDMs)

Peripheral blood mononuclear cells (PBMCs) were isolated from buffy coats derived from healthy subjects and received by ARNAS "Civico, Di Cristina, Benfratelli" (Palermo, Italy) according to a Material Transfer Agreement signed on 8/11/2019. Human macrophages were obtained by culturing PBMCs for 7 days in complete RPMI 1640 medium (Euroclone, Milan- Italy, #ECB9006L), supplemented with 10 % fetal bovine serum (FBS, Euroclone, Milan- Italy, #ECS5000L) and 50 ng/mL of human M-CSF (Miltenyi Biotec, Bergisch Gladbach-Germany, #130-096-493). The medium was replaced after 3 days of culture. The day before each experiment, hMDMs were treated with trypsin-EDTA for 5 min, scraped, plated in a complete medium without M-CSF into 96-well plates (5×10^4 cells/well), and incubated at 37 °C and 5 % CO_2. On the day of an experiment, the culture medium was changed to 1 % FBS, and cells were stimulated with 1 μg mL^{-1} Lipopolysaccharides (LPS, from Escherichia coli 0111:B4, #L3012, Sigma-Aldrich). After 24 h, cell supernatants were collected, centrifuged at 12,000 rpm for 5 min to remove cellular debris, and stored at − 20 °C until analysis. The collected samples were diluted in PBS with ratios 1:1000 and 1:10,000 for supernatants of untreated and LPS-treated cells, respectively. Thus, 5 μL of diluted supernatant solutions were drop-casted onto a chip and incubated for 30 min at room temperature. The same culture medium

sample was also analyzed by ELISA (Enzyme-Linked Immunosorbent Assay) for the detection of H-IL8. ELISA was performed following the manufacturer's instructions (R&D Systems, #DY208).

2.5. Real saliva sample analysis

Saliva samples were obtained from one healthy volunteer using the spitting method [33], which involves gathering saliva from the front of the mouth and spitting it into a tube. Participant was instructed not to eat or drink for 30 min before saliva sample collection. The collected samples were then used as a matrix, into which H-IL8 was spiked at known concentrations. Thus, a volume of 5 μL of spiked saliva solution was drop-casted onto the chip and incubated for 30 min at room temperature.

3. Results and discussion

3.1. Microchip and electrode fabrication

The microchip device used for the immunosensor assembling was selected as it enabled multiplexed detection and fast parallel incubation onto the three WEs. The reproducibility of the microfabricated microelectrodes was first evaluated via cyclic voltammetry. The $Fe(CN)_6^{3-/4-}$ oxidation peak current values measured on the three WEs of the same chip were compared to evaluate on-chip reproducibility. To evaluate on-wafer reproducibility, peak current values measured with the same electrode across various chips selected from the same silicon wafer were compared. The results demonstrated that the fabrication procedures led to a reproducible substrate, with deviations lower than 4 %.

Gold foam was deposited on each WE of the chip via hydrogen template deposition that permitted the formation of metallic nanostructures without the use of an external template [34]. In this method, the vigorous H_2 bubbling, obtained for both the very acid solution used and the high reached cathodic potential, drove the concomitant gold deposition. As shown in the SEM images reported in Fig. 2a–c, the gold deposit assumed a nanostructured, porous morphology resembling a foam. The parameters used to reproducibly produce the gold foam deposition were selected from the results reported in [34]. The porous morphology of the foam led to an increased surface area compared to a bare gold electrode. This is qualitatively shown in the cyclic voltammetry graph of Fig. 2d. The $Fe(CN)_6^{3-/4-}$ peaks are 2.3 times higher than those obtained using bare electrode. In Fig. 2e, a linear relationship between the current peaks and the square root of the scan rate was shown. Using the Randles-Sevcik equation, it was possible to calculate the increase of the active surface area after foam deposition:

$$Ip = 2.69 \times 10^5 A \times D^{1/2}\, n^{3/2}\, v^{1/2} C$$

where Ip is the peak current, A is the surface area, D is the diffusion coefficient, n is the number of electrons of the reaction, v is the scan rate, and C is the redox species concentration. From this equation, the calculated surface area was 0.0197 mm^2, 2.5 times higher than the geometrical areas.

The next step for immunosensor substrate fabrication is deposition of an antifouling gel onto the gold foam WEs. Chitosan has been widely investigated for its antifouling properties [35], due to its ability to form a thin, uniform film that acts as a protective barrier between the electrode surface and fouling agents [36]. Its hydrophilic nature further enhances its effectiveness by promoting interactions with water molecules, thus reducing the adhesion of unwanted biomolecules [37]. BSA is also recognized for its antifouling properties and is commonly used to block surfaces to prevent non-specific protein adsorption [38]. In this study, we employed a combined approach that leverages the synergistic effects of both chitosan and BSA through an electrochemical co-deposition process. Moreover, the electrodeposition bath was supplemented with graphene oxide (GO), which was electrochemically reduced to form reduced graphene oxide (rGO). This method was chosen

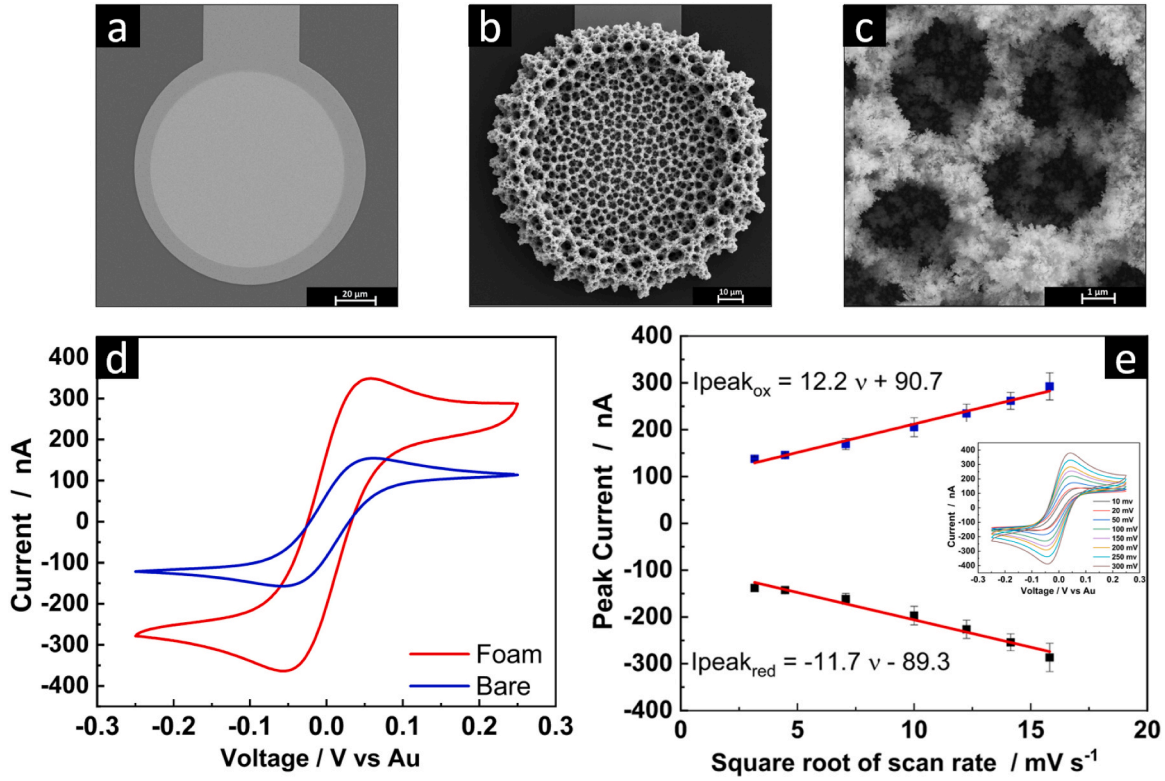

Fig. 2. SEM images of: a) bare working electrode; b–c) gold foam on the working electrode. d) CV obtained in the probe redox solution carried out before and after the Au foam deposition; e) Oxidation and reduction peak current vs scan rates performed on working electrode after gold foam deposition. Error bars represent the SD of three measurements.

because rGO, in conjunction with chitosan and BSA, provides functional groups that covalently anchor Protein A/G onto the electrode, enabling site-specific antibody immobilization.

In particular, the co-deposition of GO, chitosan, and BSA was undertaken by scanning voltammetry from 0 V to − 1.1 V. These one-step deposition conditions led to the formation of a gel layer that covered the gold foam without changing their nanostructured morphology or filling the pores, as demonstrated in Fig. 3a SEM image and better in the higher magnification image of Fig. 3b. To evaluate the change in electrode composition, EDS analysis (Fig. 3c) was performed. For comparison also, the bare and foam electrodes were analyzed. Gold and silicon peaks can be seen in all spectra. Gold peaks were from both the bare electrode and the foam, while the silicon peak is due to the silicon wafer used as the initial substrate. The carbon peak can be observed in the spectrum measured after the deposition of the antifouling layer based on Cs/rGO/BSA.

The effectiveness of carbon-based material deposition is demonstrated through the Raman analysis presented in Fig. 3d. In this spectrum, the presence of GO was confirmed by the presence of D and G bands (1346 and 1600 cm^{-1}, respectively) of GO. Also, the 2D (at 2772 cm-1) band was present but with low intensity. The intensity ratio of the D-band to the G-band (I_D/I_G) is commonly used to calculate the density of defects in sp2 carbon atoms. This ratio typically increases when the degree of GO reduction increases [39]. We measured a value of I_D/I_G ratio of about 0.98, which could be attributed to the GO reduction during the antifouling co-deposition. Furthermore, a defective structure was confirmed by the existence of 2D band (2945 cm^{-1}) [40]. Due to the very high intensity of D and G bands on the Raman spectrum, it was difficult to observe chitosan and BSA characteristic bands. This result is in agreement with other literature works concerning the study of GO composite materials [41,42].

3.2. Immunosensor assembling and performance

The immunosensor manufacturing procedure is summarized in Fig. 4a. After substrate manufacturing (Step 1), several incubation steps are required to immobilize biomolecules on the electrode surface. DPV measurements were performed after each biomolecule immobilization step (Fig. S1). Each step has a specific function, and the materials used have been carefully selected. The Cs/rGO/BSA coating (Step 2) was useful for its antifouling and biocompatibility properties, and for easier biomolecule immobilization on the gold foam surface. The antifouling performance of the CS/rGO/BSA layer was evaluated using DPV by monitoring changes in the oxidation peak current of the $Fe(CN)_6^{3-/4-}$ redox couple before and after exposure to a complex fouling matrix (specifically, undiluted human serum). The response of electrodes modified with only Au foam was compared to that of electrodes incorporating the antifouling CS/rGO/BSA layer. As shown in Fig. 5a, bare Au foam exhibited a reduction in the $Fe(CN)_6^{3-/4-}$ oxidation peak height of 21.3 ± 6.5 % after 30 min of incubation in human serum. In contrast, electrodes coated with the antifouling CS/rGO/BSA layer showed only a minor decrease of 5.9 ± 1.2 % under identical conditions. These results clearly demonstrate the effectiveness of the CS/rGO/BSA layer as an antifouling strategy, enabling minimal electrode fouling during exposure to complex biological matrices.

Surface activation with glutaraldehyde (Step 3) is a reliable approach for immobilizing bioreceptors such as antibodies [43], enzymes [44], DNA [45], and so on. For these reasons, the -NH_2 functional groups of the chitosan-based antifouling coating were activated by overnight incubation with 1.5 % glutaraldehyde (Fig. 4b).

The A/G protein (Step 4) was utilized as a mediator to prevent the random immobilization of antibodies on the electrode surface. All the ammine groups on the antibody, including those in the Fc region and

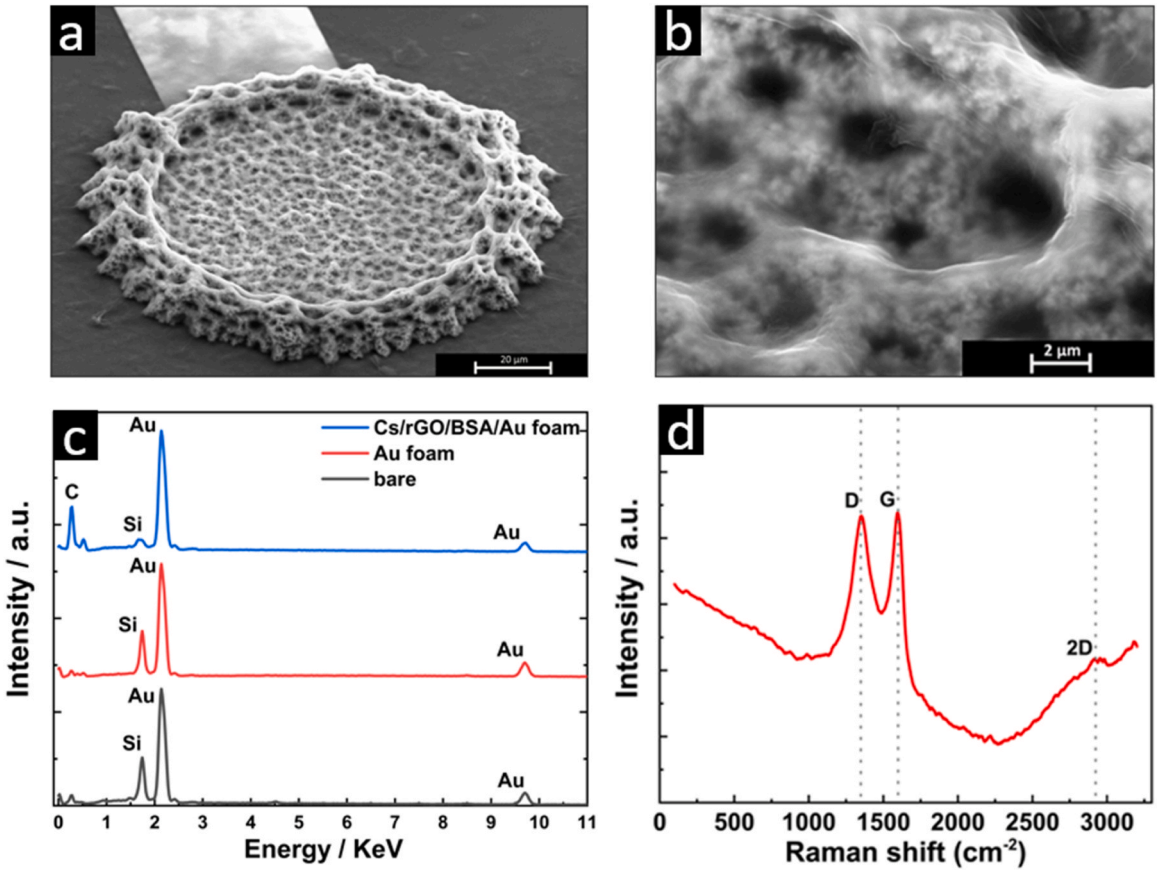

Fig. 3. a–b) SEM images of Cs/rGO/BSA modified electrode, c) EDS of working electrode (Bare, after Au foam deposition, after Cs/rGO/BSA deposition); d) Raman spectrum of Cs/rGO/BSA/Au foam electrode.

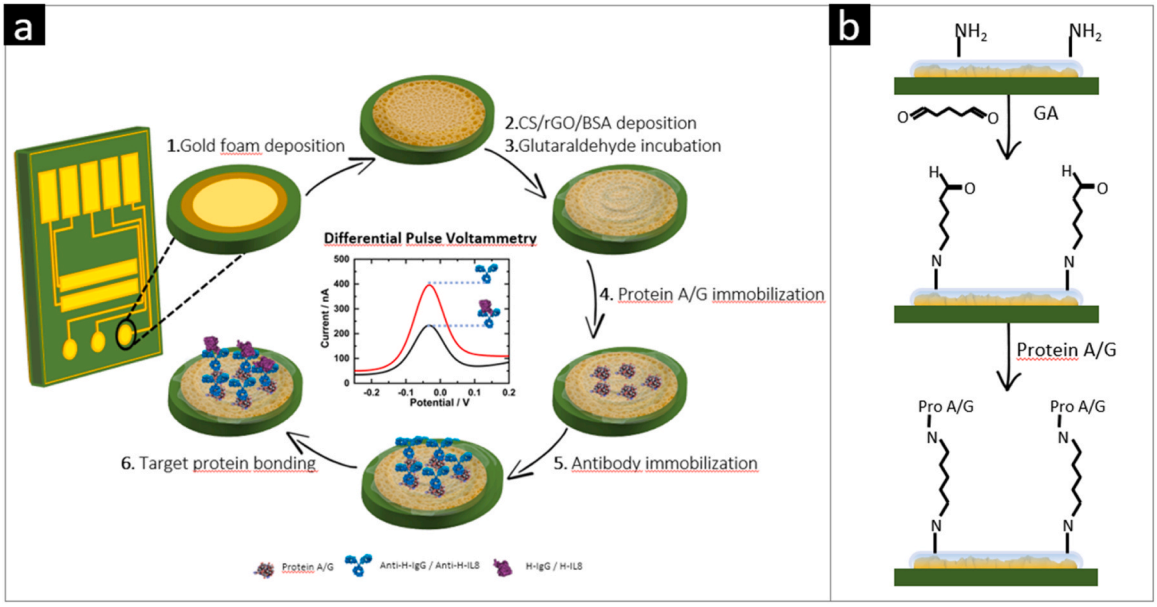

Fig. 4. a) Immunosensor fabrication scheme; b) Glutaraldehyde surface activation reaction mechanism.

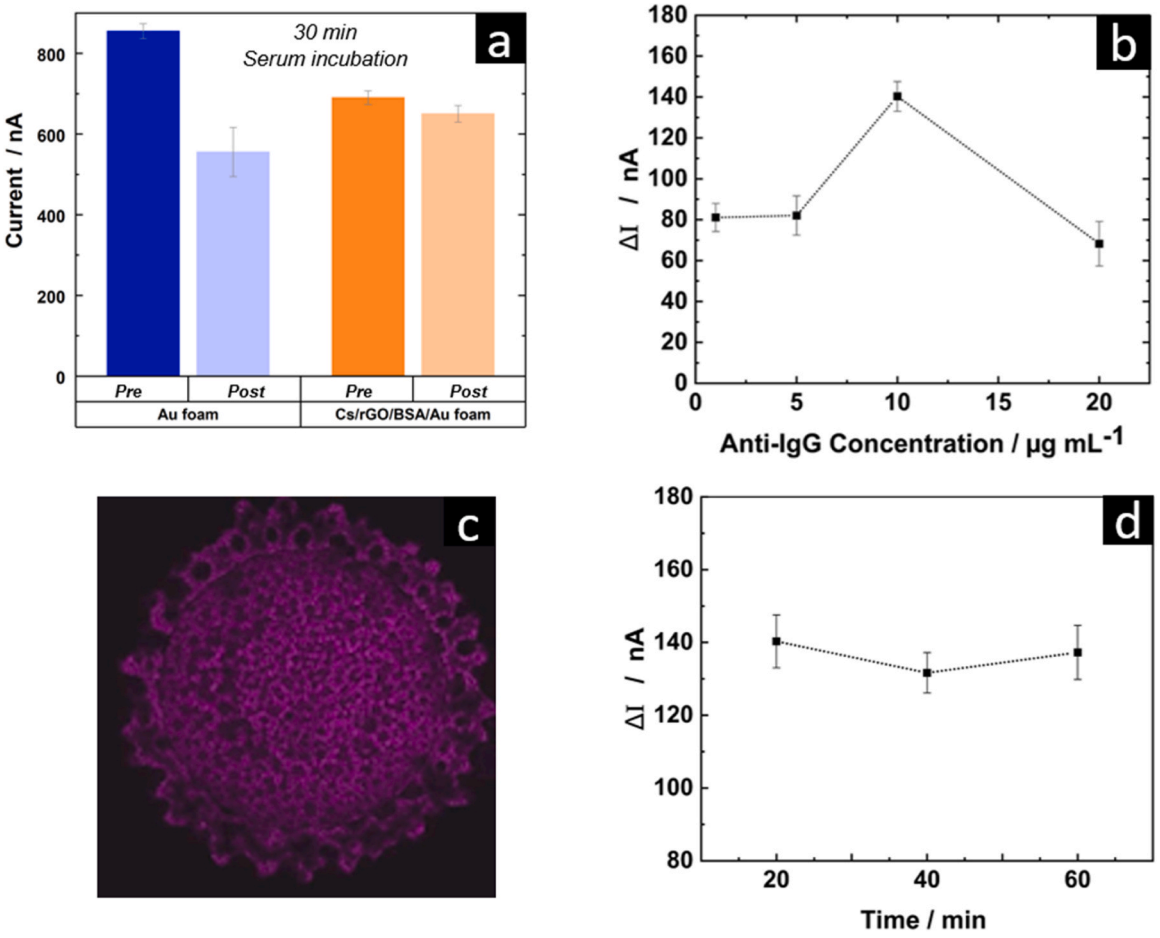

Fig. 5. a) Oxidation peak heights of $Fe(CN)_6^{3-/4-}$ obtained by DPV for Au foam and for electrodes modified with the antifouling CS/rGO/BSA layer, before and after 30 min of incubation in human serum; b) Anti-H-IgG concentration on the sensor response; c) Immunosensor CLSM image after antibody incubation; d) Effect of the Blocking time on sensor response. DPV sensor response was measured after 10 pg mL^{-1} H-IgG incubation in PBS probe solution. Error bars represent the SD of six measurements.

antibody-binding Fab regions, can bind covalently to the activated surface. Therefore, in addition to the upright end-on position, in which the binding sites are exposed and free to bind, the antibody can also bind in the side-on and head-on positions. In the latter case, the target protein binding sites are no longer available, lowering the sensor sensitivity [44]. The role of A/G protein is to remove the random immobilization and orientation. A/G protein contains the Fc-binding domains of proteins A and G, where the antibodies can bind with an end-on position [46,47]. Additionally, protein A/G has a high affinity for binding human IgG antibodies [48]. Electrochemical characterization was first employed to monitor surface modification after protein A/G immobilization. As shown in Fig. S1, a clear decrease in peak current was observed after incubation with protein A/G, indicating partial hindrance of electron transfer due to the presence of the protein layer. This result supports the successful attachment of protein A/G to the electrode surface. Further confirmation was obtained by FTIR spectroscopy. To clearly identify protein-specific signals, BSA was excluded from the Cs/rGO/BSA deposition bath to avoid spectral overlap. As shown in Fig. S2, the FTIR spectrum of Cs/rGo/Protein A/G modified electrode exhibits characteristic absorption bands corresponding to the amide I (1600–1700 cm^{-1}), amide II (1470–1570 cm^{-1}), and amide III (1220–1320 cm^{-1}) [49]. The presence of these bands confirms not only the successful immobilization of Protein A/G but also the preservation of its structural integrity upon surface binding. Additionally, a peak at 1070 cm^{-1}, attributable to the P–O asymmetric stretching vibration, was detected. This signal likely originates from residual phosphate of PBS buffer used during the protein A/G incubation step. It is worth noting that the FTIR spectrum appears relatively noisy, which can be attributed to the thinness of the Cs/rGO film and the inherent structural defects of reduced graphene oxide (rGO). These defects can lead to peak shifts, variations in relative intensity, and the suppression of certain signals [50], complicating spectral interpretation. Nonetheless, the key characteristic peaks of chitosan and rGO are identified and summarized in Table S1, confirming the presence of the expected functional groups within the composite matrix.

After A/G protein incubation, the sensor was ready for the antibody immobilization step (Step 5). The antibody concentration was optimized by measuring sensor response to 10 pg mL^{-1} H-IgG and varying the anti-H-IgG concentration in the range from 1 to 20 μg mL^{-1}. The current response of the sensor, ΔI, increased with the increasing antibody concentration until reaching a maximum value at 10 μg mL^{-1}, Fig. 5b, and then decreased again. This trend was due to the gradual coverage of the electrode surface, which, therefore, can be considered completely covered at 10 μg mL^{-1} [51,52]. Thus, this antibody concentration was selected as the optimal value for the fabrication of the immunosensor. To verify the efficacy of antibody immobilization, fluorescence microscopy analysis was carried out. In this process, anti–H–IgG was replaced with a fluorescent-tagged antibody (Donkey anti–Rabbit–IgG, Alexa Fluor™ 647) and the electrode was examined using CLSM, Fig. 5c. The CLSM image of the electrode surface after the incubation with fluorescent-tagged antibodies revealed a uniform distribution of the fluorescent tag. Thus, the antibodies are uniformly attached to the electrode surface, suggesting the success of the developed immobilization procedure.

Before incubating with the analyte, an immunosensor-activated surface was treated with a blocking agent to cover all remaining active sites on the surface to avoid non-specific binding. The Superblock®, often used in ELISA, was selected because of its ability to quickly block the surface (Step 6) [53,54]. The effect of blocking time incubation was studied, evaluating the sensor response to 10 pg mL^{-1} of H-IgG. In Fig. 5d, it can be observed that the sensor response is practically independent of the blocking time. Thus, a blocking incubation time of 20 min was selected to continue the fabrication. All optimizations utilized the protein H-IgG as the target. However, the replacement of the H–IgG antibody with one of different specificity while maintaining the same isotype makes it possible to use the immunosensor for other targets. In this study, two different targets were used to demonstrate the potential for H-IgG and H-IL8 multiplexed detection (Step 7). This was possible by immobilizing different antibodies on each chip electrode, specifically Anti-H-IgG in electrode E1 and Anti-H-IL8 in E3.

The optimized conditions were used for the fabrication of several immunosensors that were incubated using different concentrations of the target protein diluted in PBS. The concentration range investigated was from 1 fg mL^{-1} to 10 pg mL^{-1}. The DPV scans in $Fe(CN)_6^{3-/4-}$, conducted before and after incubation with the H-IgG target, revealed antigen-antibody binding, as indicated by the decrease in the oxidation peak current after incubation, Fig. 6a. The detection principle in the proposed immunosensor is based on monitoring changes in electron transfer resistance at the electrode surface resulting from specific biorecognition processes. Antibodies immobilized on the working electrode surface form a selective interface able to capture the target protein. When incubated with the target protein, specific antigen-antibody binding occurs on the electrode surface, leading to the formation of an insulating biolayer. This insulating layer hinders electron transfer between the redox probe in solution and the electrode surface. As a result, the oxidation peak measured by DPV decreased with increasing target concentration. This decrease in current is directly linked to the degree of the surface coverage by the target protein. In Fig. 6b, the analytical signal is represented as ΔI, calculated as the difference between the oxidation peak current measured before and after incubation with the target protein. The observed increase in ΔI with rising analyte concentration reflects the progressive formation of the insulating biolayer and confirms the sensor ability to quantitatively detect the target protein. For H-IgG target, the sensor was sensitive to very low concentrations, while for values higher than 1 pg mL^{-1} saturation was reached, indicating that antibodies binding sites were entirely covered. Due to the Hook's effect, a slight decrease was observed at 10 pg mL^{-1} [55,56]. This phenomenon occurs for very high amounts of analyte. Under these conditions, the antigen molecules sterically hinder each other from reaching the binding sites of the antibody, resulting in a decrease in signal. For H-IgG target, a linear response in the range from 10 fg mL^{-1} to 1 pg mL^{-1} was found, Fig. 6c, with a sensitivity of 73.94 of nA mL pg^{-1}. The following equation was used to calculate the LOD of the sensor:

$$LOD = 3\sigma/S$$

where σ is the standard deviation of blank measurements, S is the sensor sensitivity, which is determined by the slope of the calibration line. A very low value of LOD was calculated, 69.2 fg mL^{-1}.

To create a multiplexed device for monitoring inflammation, the above process was repeated to develop a sensor for H–IL8 detection. The same parameters optimized for H-IgG detection were used to fabricate the H-IL8 sensor, with Anti–H-IL8 immobilized on the electrode surface. As shown by the calibration line in Fig. 6d, the immunosensor exhibited a calibration curve similar to that of H-IgG, with a sensitivity of 83.57 nA mL pg^{-1} across a linear range from 10 fg mL^{-1} to 1 pg mL^{-1} and a LOD of 87.6 fg mL^{-1}. The versatility of the developed method was thus demonstrated, as no significant differences were observed when replacing the model analyte H-IgG with the cytokine, by simply modifying the immobilized antibody accordingly. For both target analytes, the observed results demonstrate that the immunosensor performed well in terms of linear range and LOD, as well as in sensitivity. This is evident from the comparison with literature data reported in Table 1. Although other studies demonstrated a wider linear range, the immunosensor fabricated in this study has a lower LOD and higher sensitivity. This is of high relevance, especially for biomedical applications.

The excellent performance demonstrated by the proposed platform opens new opportunities for potential real-world applications in cytokine detection. In this context, a comparison with the conventional ELISA method, still considered the gold standard for protein quantification, can be particularly useful to highlight the strengths of the present approach. While ELISA is a widely validated and sensitive technique, it

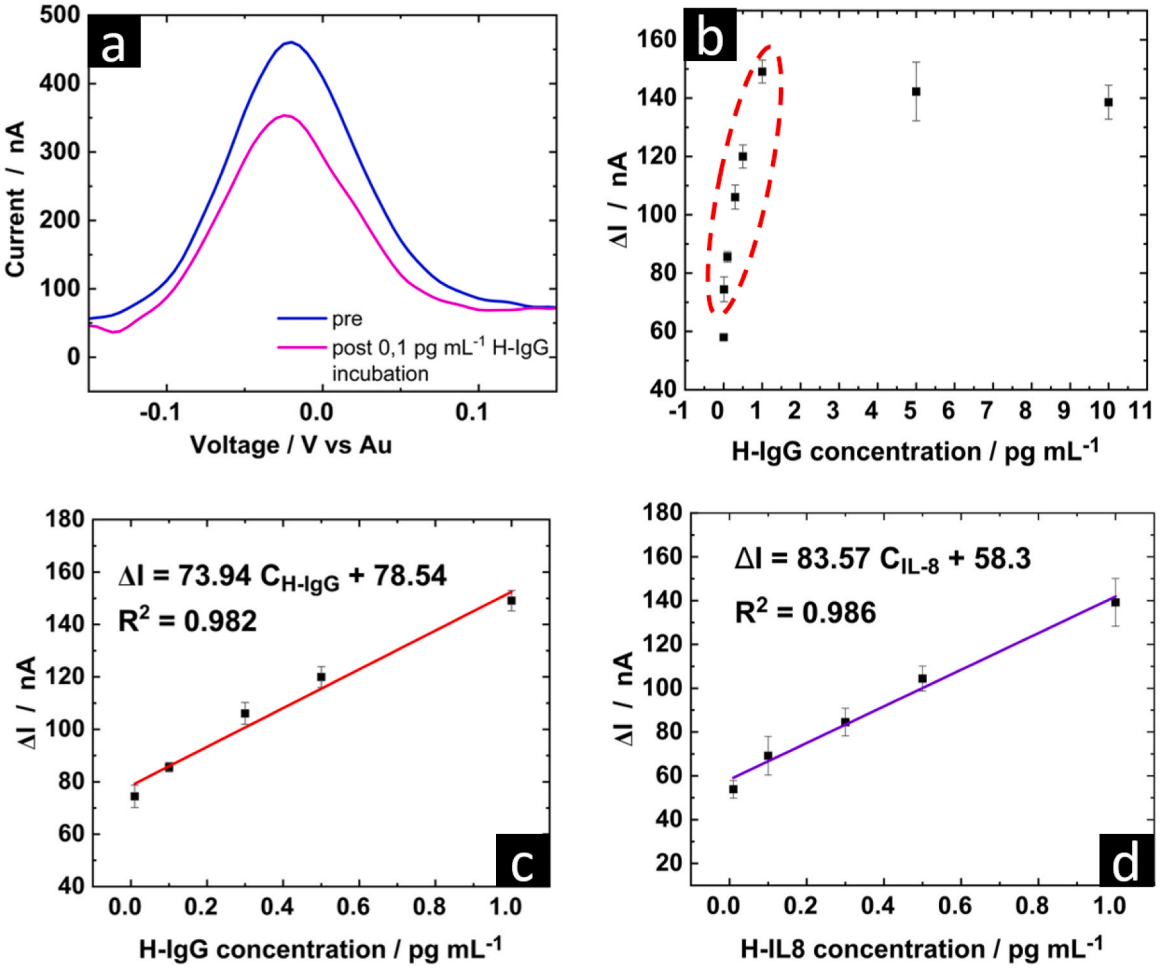

Fig. 6. a) DPV before and after 0,1 pg mL^{-1} H-IgG incubation; b) Immunosensor response at different H-IgG concentrations; c) Calibration line obtained for H-IgG.; d) Calibration line obtained for H-IL8. DPV measurements were performed in probe solution. Error bars represent the SD of five measurements.

Table 1
Comparison table of the proposed immunosensor and other recent work in literature.

SUBSTRATE	TARGET (MATRIX)	TECHNIQUE	LINEAR RANGE	SENSITIVITY	LOD	REF.
CARBON SPE	H-IgG (PBS)	DPV	2.5–100 ng mL^{-1} (Log)	1.7445 μA mL ng^{-1} cm^{-2}	1.99 ng mL^{-1}	[57]
PEP/DBMH/GCE	H-IgG (PBS)	DPV	0.1–10^4 ng mL^{-1}	3.296 μA mL ng^{-1}	23 pg/mL	[58]
GCE/PEDOT-CITRATE	H-IgG (PBS)	DPV	0.1–10000 ng mL^{-1}	-	0.032 ng mL^{-1}	[59]
PTH-MB/GNP	H-IgG (PBS)	DPV	10–10^4 ng mL^{-1} (Log)	12.52 μA mL ng^{-1}	3 ng mL^{-1}	[60]
SiO2/Au/GOx	H-IgG (Glucose-PBS)	CV	5–960 μM	0.07 μA L mol^{-1}	50 μM	[61]
AuNPs-rGO/ITO	IL8 (PBS and spiked human Saliva)	DPV	0.5–4000 pg mL^{-1}	7 nA mL pg^{-1}	72.73 pg mL^{-1}	[62]
MoS2/ZnO/GCE	IL8 (PBS and spiked human serum)	DPV	500–4500 pg mL^{-1}	-	11.6 fM	[63]
β-Ag2MoO4/ITO	IL8 (PBS and spiked human serum)	DPV	10^{-6}–40 ng mL^{-1}	7.03 μA ng to 1 mL cm^{-2}	90 pg mL^{-1}	[64]
CS/rGO/BSA Au FOAM	**H-IgG** (PBS, artificial saliva and human serum)	**DPV**	**0.010–1 pg mL^{-1}**	**73.94 nA mL pg^{-1}**	**69.2 fg mL^{-1}**	**This work**
CS/rGO/BSA Au FOAM	**IL8** (PBS and spiked human saliva)	**DPV**	**0.010 – 1 pg mL^{-1}**	**83.57 nA mL pg^{-1}**	**87.6 fg mL^{-1}**	**This work**

involves multiple incubation and washing steps, as well as the use of secondary antibodies and enzymatic labels and requires laboratory-based instrumentation (e.g., microplate readers). Furthermore, the total assay time typically ranges from 3 to 5 h. In contrast, the electrochemical immunosensor developed here operates in a label-free configuration, eliminating the need for a secondary antibody and reducing the overall number of procedural steps. Although some incubation and washing steps remain necessary, the overall protocol is substantially simplified. In addition to shorter assay times, the platform provides high sensitivity, significantly greater than that of conventional ELISA, which typically exhibits LOD in the low pg/mL range, as well as good reproducibility and compatibility with miniaturized formats,

making it a promising alternative to traditional immunoassays.

The selectivity of the developed immunosensor was evaluated by monitoring its performance in complex biological fluids. For this purpose, two complex matrices, artificial saliva and human serum, were used. Figs. 7a and 7b show the H-IgG calibration curves obtained in artificial saliva and human serum, respectively. Fig. 7c displays a comparison of the blank negative controls and shows that the signal at baseline in artificial saliva is higher, possibly due to matrix effects. Despite this, the sensor performed well, as shown in Fig. 7a, with a sensitivity of 41.42 nA mL pg^{-1} and a LOD of 77.1 fg mL^{-1}. In contrast, the negative control in human serum had a ΔI similar to that found in PBS. Additionally, the calibration line in Fig. 7b displayed the same slope. The successful operation of the sensor in undiluted human serum without the need for dilution highlights the effectiveness of the antifouling layer. This result highlights the CS/rGO/BSA layer ability to prevent interference and maintain sensor performance in complex biological fluids. The same chitosan antifouling effect was obtained in [58].

Before proceeding with simultaneous detection and evaluating the device efficacy as a multianalyte sensor, cross-reactivity between the two analytes was assessed. Immunosensors for H–IgG and H–IL8 were assembled separately. The cross-reactivity was evaluated by measuring the sensor output obtained by a) the blank, b) the target analyte, c) the other protein and d) by both the target and the other protein. For example, a chip was incubated with H-IgG antibodies and was tested with blank, 0.5 pg mL^{-1} of H-IgG, 0.5 pg mL^{-1} of H-IL8 and 0.5 pg mL^{-1} of both H-IgG and H-IL8. A similar approach was used to evaluate the cross-reactivity for H-IL8. As shown in Fig. 8a–b, both immunosensors exhibited no significant change in the blank signal after the addition of the other analyte of interest. In addition, immunosensors responded to a 0.5 pg mL^{-1} analyte concentration identically, even in the presence of the other analyte. This confirmed the absence of cross-reactivity effects between the immunosensors, allowing for simultaneous analyte detection. The possibility of using this sensor to simultaneously quantify the two analytes was evaluated by modifying the three on-chip electrodes with different antibodies. Specifically, E1 electrode was modified with Anti–H–IgG, while E3 with Anti–H–IL8. The efficacy of multiple analysis was evaluated by adding both analytes to the array and varying the concentration. Tests were performed using high concentrations of H-IgG (1 pg mL^{-1}) in the presence of low concentrations of H-IL8 (0.1 pg mL^{-1}) and vice versa, and also at equal concentrations (0.5 pg mL^{-1}). Fig. 8c compares measurements taken under simultaneous conditions with those obtained for each analyte individually. According to this study, the device successfully detected both biomarkers with a negligible effect of the presence of the other analyte.

3.3. Real samples

The immunosensor was then used to measure H-IL8 release from human macrophages stimulated with the proinflammatory bacterial LPS, known to induce a potent release of H-IL8. As expected, high amounts of H-IL8, in the ng mL^{-1} range, were released, as measured by ELISA. This made it necessary to proceed with sample dilution, $1:10^3$ for the untreated (NT) and $1:10^5$ for the LPS-treated cell culture. The high sensitivity and very low LOD of the immunosensor allowed measurements to be performed at optimal pH conditions and reduced potential interference due to the high sample dilution. Since these dilutions were made in PBS, concentration measurements were taken using the calibration curve obtained in PBS. The results, shown in Fig. 9d, present the analysis of three different experimental replicates. The immunosensors analysis showed an increase in H-IL8 concentration in the supernatants collected from the LPS-treated cultures (violet bar) compared to the untreated cultures (green bar). In addition, these measurements agree perfectly with the concentrations obtained using the ELISA (light violet and light green bars). Fig. 9b also shows a direct comparison between the H-IL8 concentration measured by ELISA and the proposed sensor. The results of the two methods have a linear correlation with an $R^2 > 0.99$ and a regression slope very close to 1, demonstrating the high accuracy of the developed immunosensor.

Finally, the suitability of the immunosensor for in vivo measurements was evaluated by measuring H-IL8 concentrations in real saliva samples. Saliva was collected from one healthy volunteer and subsequently spiked with known H–IL8 concentrations. The results, detailed in Table 2, showed an excellent recovery.

4. Conclusions

In this work, we developed an electrochemical multiplex immunosensor platform utilizing gold microdisk electrodes modified with gold foam and an antifouling polymeric layer. The device, comprised three gold disc working electrodes fabricated via lithography, metal evaporation and lift-off, enabled simultaneous analyses of two analytes. Electrodes were first coated with gold foam by hydrogen bubble template electrochemical deposition, followed by the application of an antifouling layer via electrochemical Cs/rGO/BSA co-deposition. This layer facilitated the site-oriented immobilization of antibodies through Protein A/G anchoring. The immunosensor demonstrated high sensitivity and low LOD for both H-IgG (69.2 fg mL^{-1}) and H-IL8 (87.6 fg mL^{-1}) in PBS, as well as in complex matrices such as human serum and artificial saliva. The chip is also able to quantify H-IL8 and H-IgG simultaneously. Its effectiveness for in vitro applications was confirmed by measuring H-IL8 concentrations in cell culture supernatants derived from human primary macrophages following treatment with the proinflammatory bacterial LPS. The results were validated for comparison using the ELISA method. Additionally, the sensor demonstrated excellent performance by accurately quantifying H-IL8 levels in spiked human saliva samples, achieving high recovery rates (≥ 94 %), thereby highlighting its suitability for real-world applications. This work highlights the platform potential for chronic inflammatory disease monitoring and its applicability for both in vitro studies as well as for the analysis of real human biological fluids.

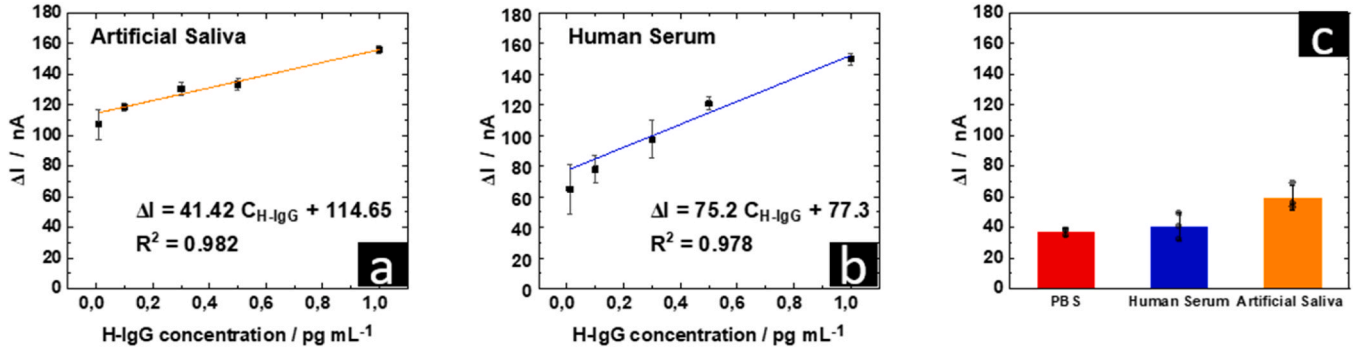

Fig. 7. Calibration line for H-IgG in a) artificial saliva and b) in human serum; c) Blanks negative control. Error bars represent the SD of five measurements.

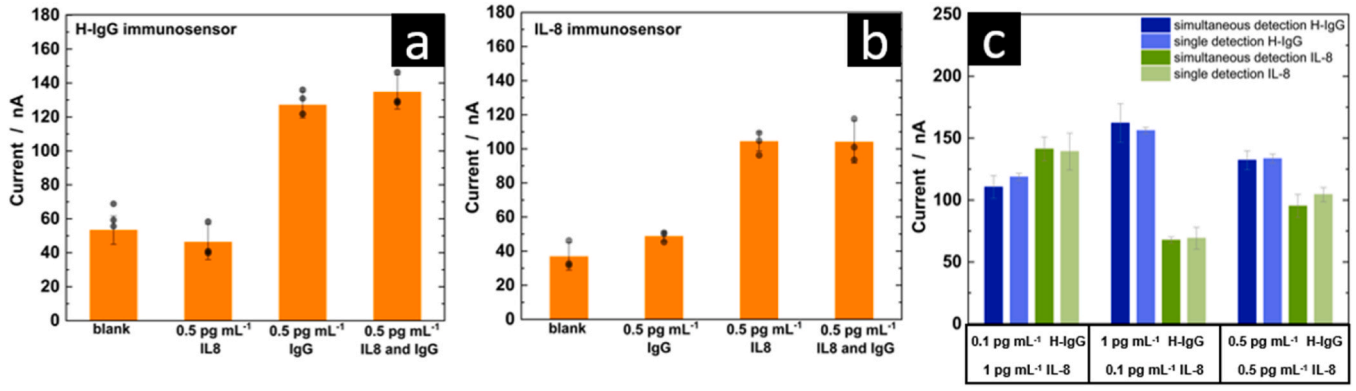

Fig. 8. a) H-IgG immunosensor response to the buffer, H-IL8, H-IgG, and H-IgG in the presence of H-IL8, b) H-IL8 immunosensor response to the buffer, H-IgG, H-IL8, and H-IL8 in the presence of H-IgG; c) multiplex immunosensor device response varying the two analytes concentrations. Error bars represent the SD of five measurements.

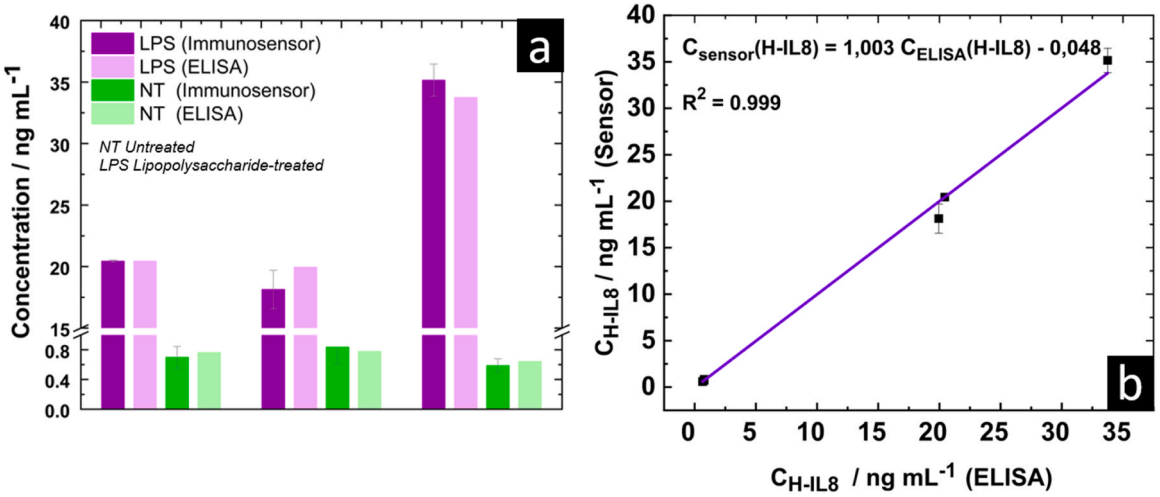

Fig. 9. a) Immunosensors response to three different pairs of cell cultures supernatants with and without LPS treatment; b) Correlation between the H-IL8 concentrations measured by the sensor and by the standard ELISA method. Error bars represent the SD of three measurements.

Table 2
Spiked saliva immunosensors measurements.

H-IL8 added [pg mL^{-1}]	H-IL8 detected [pg mL^{-1}]	RSD %	Recovery %
0	0		
0.1	0.0944	7	94
1	0.9692	4	97

CRediT authorship contribution statement

Nadia Moukri: Writing – original draft, Methodology, Investigation, Data curation. **Vuslat Juska:** Writing – review & editing, Visualization, Supervision, Methodology, Conceptualization. **Bernardo Patella:** Writing – review & editing, Supervision, Methodology, Data curation, Conceptualization. **O'Riordan Alan:** Writing – review & editing, Visualization, Supervision, Resources, Funding acquisition, Conceptualization. **Rosalinda Inguanta:** Writing – review & editing, Visualization, Supervision, Resources, Project administration, Funding acquisition. **Maria Rita Giuffrè:** Writing – review & editing, Methodology, Investigation, Data curation. **Elisabetta Pace:** Writing – review & editing, Visualization, Supervision, Conceptualization. **Chiara Cipollina:** Writing – review & editing, Visualization, Supervision, Conceptualization.

Declaration of Competing Interest

The authors declare that they have no known competing financial interests or personal relationships that could have appeared to influence the work reported in this paper.

Acknowledgments

This work was supported by University of Palermo, Ri.MED Foundation and Italian National Research Council, and has been partially financed by the Project "PATCHES – Patient-Centered HEalthcare System for Neurodegenerative Diseases" (n. 610, Ministero dello Sviluppo Economico, Accordi per l'innovazione, Programma operativo nazionale « Imprese e competitività» 2014–2020 FESR e del Fondo per la crescita sostenibile) and has emanated in part with the financial support of Research Ireland and the Department of Agriculture, Food and Marine on behalf of the Government of Ireland under Grant no. 21/RC/10303_P2 - VistaMilk. The silicon devices are designed by Dr. Juska (Tyndall National Institute Internal Catalyst Grant (ICA1920)).

Appendix A. Supporting information

Supplementary data associated with this article can be found in the online version at doi:10.1016/j.snb.2025.138604.

Data availability

No data was used for the research described in the article.

References

[1] G. Maduraiveeran, W. Jin, Functional nanomaterial-derived electrochemical sensor and biosensor platforms for biomedical applications, in: Handbook of Nanomaterials in Analytical Chemistry, Elsevier, 2020, pp. 297–327, https://doi.org/10.1016/B978-0-12-816699-4.00012-8.

[2] D. Furman, J. Campisi, E. Verdin, P. Carrera-Bastos, S. Targ, C. Franceschi, L. Ferrucci, D.W. Gilroy, A. Fasano, G.W. Miller, A.H. Miller, A. Mantovani, C. M. Weyand, N. Barzilai, J.J. Goronzy, T.A. Rando, R.B. Effros, A. Lucia, N. Kleinstreuer, G.M. Slavich, Chronic inflammation in the etiology of disease across the life span, Nat. Med. 25 (2019) 1822–1832, https://doi.org/10.1038/s41591-019-0675-0.

[3] G. Ferrante, S. La Grutta, The burden of pediatric asthma, Front. Pedia 6 (2018) 186, https://doi.org/10.3389/fped.2018.00186.

[4] Y. Meng, Q. Ji, A. Zhang, Y. Zhan, Trends in the prevalence and incidence of chronic obstructive pulmonary disease among adults aged ≥ 50 years in the United States, 2000–2020, Chronic Dis. Transl. Med. 10 (2024) 302–311, https://doi.org/10.1002/cdt3.135.

[5] G. Viegi, S. Maio, S. Fasola, S. Baldacci, Global burden of chronic respiratory diseases, J. Aerosol Med. Pulm. Drug Deliv. 33 (2020) 171–177, https://doi.org/10.1089/jamp.2019.1576.

[6] B.S. Qazi, K. Tang, A. Qazi, Recent advances in underlying pathologies provide insight into Interleukin-8 expression-mediated inflammation and angiogenesis, Int. J. Inflamm. 2011 (2011) 1–13, https://doi.org/10.4061/2011/908468.

[7] A. Ray, Cytokines and their role in health and disease: a brief overview, MOJI 4 (2016), https://doi.org/10.15406/moji.2016.04.00121.

[8] I.D. Pavord, S. Korn, P. Howarth, E.R. Bleecker, R. Buhl, O.N. Keene, H. Ortega, P. Chanez, Mepolizumab for severe eosinophilic asthma (DREAM): a multicentre, double-blind, placebo-controlled trial, Lancet 380 (2012) 651–659, https://doi.org/10.1016/S0140-6736(12)60988-X.

[9] M. Rabahi, A.P. Junqueira-Kipnis, M.R. Moraes, K. Correa, A. Castro Da Costa, Interleukin-6 and interleukin-8 blood levels' poor association with the severity and clinical profile of ex-smokers with COPD, COPD (2014) 735, https://doi.org/10.2147/COPD.S64135.

[10] F. Ricci, G. Adornetto, G. Palleschi, A review of experimental aspects of electrochemical immunosensors, Electrochim. Acta 84 (2012) 74–83, https://doi.org/10.1016/j.electacta.2012.06.033.

[11] H. Sohrabi, H. kholafazad Kordasht, P. Pashazadeh-Panahi, P. Nezhad-Mokhtari, M. Hashemzaei, M.R. Majidi, J. Mosafer, F. Oroojalian, A. Mokhtarzadeh, M. de la Guardia, Recent advances of electrochemical and optical biosensors for detection of C-reactive protein as a major inflammatory biomarker, Microchem. J. 158 (2020) 105287, https://doi.org/10.1016/j.microc.2020.105287.

[12] Y. Yang, W. Gao, Wearable and flexible electronics for continuous molecular monitoring, Chem. Soc. Rev. 48 (2019) 1465–1491, https://doi.org/10.1039/C7CS00730B.

[13] Y. Wu, C. Wang, C. Wang, P. Wang, X. Chang, L. Han, Y. Zhang, Multiple biomarker simultaneous detection in serum via a nanomaterial-functionalized biosensor for ovarian tumor/cancer diagnosis, Micromachines 13 (2022) 2046, https://doi.org/10.3390/mi13122046.

[14] S. Kongkaew, S. Cotchim, P. Kanatharana, P. Thavarungkul, W. Limbut, Disposable label-free electrochemical immunosensor based on prussian blue nanocubes for four breast cancer tumor markers, Talanta 255 (2023) 124229, https://doi.org/10.1016/j.talanta.2022.124229.

[15] V.B. Juska, G. Maxwell, P. Estrela, M.E. Pemble, A. O'Riordan, Silicon microfabrication technologies for biology integrated advance devices and interfaces, Biosens. Bioelectron. 237 (2023) 115503, https://doi.org/10.1016/j.bios.2023.115503.

[16] S.B. Nimse, M.D. Sonawane, K.-S. Song, T. Kim, Biomarker detection technologies and future directions, Analyst 141 (2016) 740–755, https://doi.org/10.1039/C5AN01790D.

[17] D. Sim, M.C. Brothers, J.M. Slocik, A.E. Islam, B. Maruyama, C.C. Grigsby, R. R. Naik, S.S. Kim, Biomarkers and detection platforms for human health and performance monitoring: a review, Adv. Sci. 9 (2022) 2104426, https://doi.org/10.1002/advs.202104426.

[18] C. Hollander, B. Sitkauskiene, R. Sakalauskas, U. Westin, S.M. Janciauskiene, Serum and bronchial lavage fluid concentrations of IL-8, SLPI, sCD14 and sICAM-1 in patients with COPD and asthma, Respir. Med. 101 (2007) 1947–1953, https://doi.org/10.1016/j.rmed.2007.04.010.

[19] M. Govoni, M. Bassi, D. Santoro, S. Donegan, D. Singh, Serum IL-8 as a determinant of response to phosphodiesterase-4 inhibition in chronic obstructive pulmonary disease, Am. J. Respir. Crit. Care Med. 208 (2023) 559–569, https://doi.org/10.1164/rccm.202301-0071OC.

[20] S. Marshall, A.J. McCann, T.L. Samuels, A. Blair, V. Bonne, N. Johnston, J. Koufman, Detection of pepsin and IL-8 in saliva of adult asthmatic patients, JAA 12 (2019) 155–161, https://doi.org/10.2147/JAA.S205482.

[21] J.M. Yoshizawa, C.A. Schafer, J.J. Schafer, J.J. Farrell, B.J. Paster, D.T.W. Wong, Salivary biomarkers: toward future clinical and diagnostic utilities, Clin. Microbiol. Rev. 26 (2013) 781–791, https://doi.org/10.1128/CMR.00021-13.

[22] B.N. Zamora-Mendoza, R. Espinosa-Tanguma, M.G. Ramírez-Elías, R. Cabrera-Alonso, G. Montero-Moran, D. Portales-Pérez, J.A. Rosales-Romo, J.F. Gonzalez, C. Gonzalez, Surface-enhanced Raman spectroscopy: a non invasive alternative procedure for early detection in childhood asthma biomarkers in saliva, Photodiagn. Photodyn. Ther. 27 (2019) 85–91, https://doi.org/10.1016/j.pdpdt.2019.05.009.

[23] F.F. Little, D.M. Delgado, P.J. Wexler, F.G. Oppenheim, P. Mitchell, J.A. Feldman, D.R. Walt, R.D. Peng, E.C. Matsui, Salivary inflammatory mediator profiling and correlation to clinical disease markers in asthma, PLoS One 9 (2014) e84449, https://doi.org/10.1371/journal.pone.0084449.

[24] C. Zhu, G. Yang, H. Li, D. Du, Y. Lin, Electrochemical sensors and biosensors based on nanomaterials and nanostructures, Anal. Chem. 87 (2015) 230–249, https://doi.org/10.1021/ac5039863.

[25] P. Malik, R. Gupta, V. Malik, R.K. Ameta, Emerging nanomaterials for improved biosensing, Meas. Sens. 16 (2021) 100050, https://doi.org/10.1016/j.measen.2021.100050.

[26] L. Bezinge, A. Suea-Ngam, A.J. deMello, C.-J. Shih, Nanomaterials for molecular signal amplification in electrochemical nucleic acid biosensing: recent advances and future prospects for point-of-care diagnostics, Mol. Syst. Des. Eng. 5 (2020) 49–66, https://doi.org/10.1039/C9ME00135B.

[27] Z. Li, G.-Y. Chen, Current conjugation methods for immunosensors, Nanomaterials 8 (2018) 278, https://doi.org/10.3390/nano8050278.

[28] N.G. Welch, J.A. Scoble, B.W. Muir, P.J. Pigram, Orientation and characterization of immobilized antibodies for improved immunoassays (review), Biointerphases 12 (2017) 02D301, https://doi.org/10.1116/1.4978435.

[29] X. Meng, Y. Xu, B. Ma, Z. Ma, H. Han, Anti-fouling materials decorated immunoprobe and electrochemical sensing interface to improve immunoassay, Chem. Eng. J. 450 (2022) 137954, https://doi.org/10.1016/j.cej.2022.137954.

[30] G. Song, H. Han, Z. Ma, Anti-fouling strategies of electrochemical sensors for tumor markers, Sensors 23 (2023) 5202, https://doi.org/10.3390/s23115202.

[31] M.J. Russo, M. Han, P.E. Desroches, C.S. Manasa, J. Dennaoui, A.F. Quigley, R.M. I. Kapsa, S.E. Moulton, R.M. Guijt, G.W. Greene, S.M. Silva, Antifouling strategies for electrochemical biosensing: mechanisms and performance toward point of care based diagnostic applications, ACS Sens. 6 (2021) 1482–1507, https://doi.org/10.1021/acssensors.1c00390.

[32] G.J. Ma, A.R. Ferhan, J.A. Jackman, N.-J. Cho, Conformational flexibility of fatty acid-free bovine serum albumin proteins enables superior antifouling coatings, Commun. Mater. 1 (2020) 45, https://doi.org/10.1038/s43246-020-0047-9.

[33] F.G. Bellagambi, T. Lomonaco, P. Salvo, F. Vivaldi, M. Hangouët, S. Ghimenti, D. Biagini, F. Di Francesco, R. Fuoco, A. Errachid, Saliva sampling: methods and devices. An overview, TrAC Trends Anal. Chem. 124 (2020) 115781, https://doi.org/10.1016/j.trac.2019.115781.

[34] V.B. Juska, S. Hendriks, E. Santillan-Urquiza, N. Moukri, P. Estrela, G.D. Maxwell, B. O'Brien, B. Patella, R. Inguanta, O'Riordan, On-chip multiplexed voltammetry using a universal antifouling hydrogel and porous gold foam interface for stress and inflammation monitoring, Adv. Sens. Res. (2025) e00198, https://doi.org/10.1002/adsr.202400198.

[35] R. Verma, C. Verma, B. Gupta, S. Mukhopadhyay, Preparation and characterization of structural and antifouling properties of chitosan/polyethylene oxide membranes, Int. J. Biol. Macromol. 278 (2024) 134693, https://doi.org/10.1016/j.ijbiomac.2024.134693.

[36] J. Li, X. Qiao, Z. Wei, Q. Yang, S. Xu, C. Li, X. Luo, An antifouling electrochemical biosensor based on chitosan and DNA dual-network hydrogel for ATP quantification in complex biofluids, Sens. Actuators B Chem. 424 (2025) 136937, https://doi.org/10.1016/j.snb.2024.136937.

[37] P.-H. Lin, B.-R. Li, Antifouling strategies in advanced electrochemical sensors and biosensors, Analyst 145 (2020) 1110–1120, https://doi.org/10.1039/C9AN02017A.

[38] W. Chen, M. Chi, M. Wang, Y. Liu, S. Kong, L. Du, J. Wang, C. Wu, Label-free detection of CA19-9 using a BSA/graphene-based antifouling electrochemical immunosensor, Sensors 23 (2023) 9693, https://doi.org/10.3390/s23249693.

[39] Y. Shen, T. Jing, W. Ren, J. Zhang, Z.-G. Jiang, Z.-Z. Yu, A. Dasari, Chemical and thermal reduction of graphene oxide and its electrically conductive polylactic acid nanocomposites, Compos. Sci. Technol. 72 (2012) 1430–1435, https://doi.org/10.1016/j.compscitech.2012.05.018.

[40] R. Muzyka, S. Drewniak, T. Pustelny, M. Chrubasik, G. Gryglewicz, Characterization of graphite oxide and reduced graphene oxide obtained from different graphite precursors and oxidized by different methods using Raman spectroscopy, Materials 11 (2018) 1050, https://doi.org/10.3390/ma11071050.

[41] A.M. Onaș, I.E. Bîru, S.A. Gârea, H. Iovu, Novel bovine serum albumin protein backbone reassembly study: strongly twisted β-sheet structure promotion upon interaction with GO-PAMAM, Polymers 12 (2020) 2603, https://doi.org/10.3390/polym12112603.

[42] V. Dhayal, S.Z. Hashmi, U. Kumar, B.L. Choudhary, A.E. Kuznetsov, S. Dalela, S. Kumar, S. Kaya, S.N. Dolia, P.A. Alvi, Spectroscopic studies, molecular structure optimization and investigation of structural and electrical properties of novel and biodegradable Chitosan-GO polymer nanocomposites, J. Mater. Sci. 55 (2020) 14829–14847, https://doi.org/10.1007/s10853-020-05093-5.

[43] M.G.R. Pimenta-Martins, R.F. Furtado, L.G.D. Heneine, R.S. Dias, M.D.F. Borges, C. R. Alves, Development of an amperometric immunosensor for detection of staphylococcal enterotoxin type A in cheese, J. Microbiol. Methods 91 (2012) 138–143, https://doi.org/10.1016/j.mimet.2012.05.016.

[44] O. Barbosa, C. Ortiz, Á. Berenguer-Murcia, R. Torres, R.C. Rodrigues, R. Fernandez-Lafuente, Glutaraldehyde in bio-catalysts design: a useful crosslinker and a versatile tool in enzyme immobilization, RSC Adv. 4 (2014) 1583–1600, https://doi.org/10.1039/C3RA45991H.

[45] Q. Wang, B. Zhang, X. Lin, W. Weng, Hybridization biosensor based on the covalent immobilization of probe DNA on chitosan–mutiwalled carbon nanotubes

nanocomposite by using glutaraldehyde as an arm linker, Sens. Actuators B Chem. 156 (2011) 599–605, https://doi.org/10.1016/j.snb.2011.02.004.
[46] S.K. Vashist, J.H.T. Luong, Antibody immobilization and surface functionalization chemistries for immunodiagnostics, in: Handbook of Immunoassay Technologies, Elsevier, 2018, pp. 19–46, https://doi.org/10.1016/B978-0-12-811762-0.00002-5.
[47] M. Shen, J.F. Rusling, C.K. Dixit, Site-selective orientated immobilization of antibodies and conjugates for immunodiagnostics development, Methods 116 (2017) 95–111, https://doi.org/10.1016/j.ymeth.2016.11.010.
[48] T. Rispens, G. Vidarsson, Human IgG subclasses, in: Antibody Fc, Elsevier, 2014, pp. 159–177, https://doi.org/10.1016/b978-0-12-394802-1.00009-1.
[49] Y. Ji, X. Yang, Z. Ji, L. Zhu, N. Ma, D. Chen, X. Jia, J. Tang, Y. Cao, DFT-Calculated IR spectrum amide I, II, and III band contributions of *n*-methylacetamide fine components, ACS Omega 5 (2020) 8572–8578, https://doi.org/10.1021/acsomega.9b04421.
[50] C. Zhang, D.M. Dabbs, L.-M. Liu, I.A. Aksay, R. Car, A. Selloni, Combined effects of functional groups, lattice defects, and edges in the infrared spectra of graphene oxide, J. Phys. Chem. C 119 (2015) 18167–18176, https://doi.org/10.1021/acs.jpcc.5b02727.
[51] S. Amarasiri Fernando, G.S. Wilson, Studies of the 'hook' effect in the one-step sandwich immunoassay, J. Immunol. Methods 151 (1992) 47–66, https://doi.org/10.1016/0022-1759(92)90104-2.
[52] A. Ahmed, J.V. Rushworth, J.D. Wright, P.A. Millner, Novel impedimetric immunosensor for detection of pathogenic bacteria *Streptococcus pyogenes* in human saliva, Anal. Chem. 85 (2013) 12118–12125, https://doi.org/10.1021/ac403253j.
[53] W. Iwasaki, C. Kataoka, K. Sawadaishi, K. Suyama, N. Morita, M. Miyazaki, A simple, low cost, sensitive, and portable electrochemical immunochromatography sensing device to measure estrone-3-sulfate, Sensors 20 (2020) 4781, https://doi.org/10.3390/s20174781.
[54] C.C. Pola, S.V. Rangnekar, R. Sheets, B.M. Szydłowska, J.R. Downing, K.W. Parate, S.G. Wallace, D. Tsai, M.C. Hersam, C.L. Gomes, J.C. Claussen, Aerosol-jet-printed graphene electrochemical immunosensors for rapid and label-free detection of SARS-CoV-2 in saliva, 2D Mater. 9 (2022) 035016, https://doi.org/10.1088/2053-1583/ac7339.
[55] A. Dasgupta, A. Wahed, Immunoassay platform and designs, in: Clinical Chemistry, Immunology and Laboratory Quality Control, Elsevier, 2014, pp. 19–34, https://doi.org/10.1016/B978-0-12-407821-5.00002-4.
[56] S. Cavalera, A. Russo, E.A. Foglia, S. Grazioli, B. Colitti, S. Rosati, C. Nogarol, F. Di Nardo, T. Serra, M. Chiarello, C. Baggiani, G. Pezzoni, E. Brocchi, L. Anfossi, Design of multiplexing lateral flow immunoassay for detection and typing of foot-and-mouth disease virus using pan-reactive and serotype-specific monoclonal antibodies: evidence of a new hook effect, Talanta 240 (2022) 123155, https://doi.org/10.1016/j.talanta.2021.123155.
[57] W. Jumpathong, J. Jakmunee, K. Ounnunkad, A sensitive and disposable graphene oxide electrochemical immunosensor for label-free detection of human immunoglobulin g, Anal. Sci. 32 (2016) 323–328, https://doi.org/10.2116/analsci.32.323.
[58] H. Yang, Q. Hou, C. Ding, Denatured bovine serum albumin hydrogel–based electrochemical biosensors for detection of IgG, Microchim. Acta 189 (2022) 400, https://doi.org/10.1007/s00604-022-05499-9.
[59] M. Chen, Z. Song, R. Han, Y. Li, X. Luo, Low fouling electrochemical biosensors based on designed Y-shaped peptides with antifouling and recognizing branches for the detection of IgG in human serum, Biosens. Bioelectron. 178 (2021) 113016, https://doi.org/10.1016/j.bios.2021.113016.
[60] L.-P. Qiu, C.-C. Wang, P. Hu, Z.-S. Wu, G.-L. Shen, R.-Q. Yu, A label-free electrochemical immunoassay for IgG detection based on the electron transfer, Talanta 83 (2010) 42–47, https://doi.org/10.1016/j.talanta.2010.08.036.
[61] D. Tang, R. Niessner, D. Knopp, Flow-injection electrochemical immunosensor for the detection of human IgG based on glucose oxidase-derivated biomimetic interface, Biosens. Bioelectron. 24 (2009) 2125–2130, https://doi.org/10.1016/j.bios.2008.11.008.
[62] S. Verma, A. Singh, A. Shukla, J. Kaswan, K. Arora, J. Ramirez-Vick, P. Singh, S. P. Singh, Anti-IL8/AuNPs-rGO/ITO as an immunosensing platform for noninvasive electrochemical detection of oral cancer, ACS Appl. Mater. Interfaces 9 (2017) 27462–27474, https://doi.org/10.1021/acsami.7b06839.
[63] C. Vetrivel, G. Sivarasan, K. Durairaj, C. Ragavendran, C. Kamaraj, S. Karthika, H.-M. Lo, MoS2-ZnO nanocomposite mediated immunosensor for non-invasive electrochemical detection of IL8 oral tumor biomarker, Diagnostics 13 (2023) 1464, https://doi.org/10.3390/diagnostics13081464.
[64] N. Pachauri, G.B.V.S. Lakshmi, S. Sri, P.K. Gupta, P.R. Solanki, Silver molybdate nanoparticles based immunosensor for the non-invasive detection of Interleukin-8 biomarker, Mater. Sci. Eng.: C 113 (2020) 110911, https://doi.org/10.1016/j.msec.2020.110911.

Nadia Moukri received her PhD in 2024, from the University of Palermo. Currently, she is a Postdoctoral Researcher at University of Palermo, Department of Engineering. Her current research interests include the development of nanostructures obtained by template electrosynthesis and via chemical deposition for the fabrication of electrochemical biosensors and immunosensors.

Vuslat Juska received her Ph.D. from University College Cork and is currently a postdoctoral fellow at the Chan Zuckerberg Biohub Chicago and Northwestern University. Her research centers on the development of electronic biointerfaces for advanced diagnostics and real-time biomolecular monitoring in biomedical applications. Her work has been recognized with several prestigious honors, including the BOC Postgraduate Award and the MSCA-Dorothy Fellowship. She has also received eleven scientific image awards across Tyndall National Institute, University College Cork, and Northwestern University.

Bernardo Patella obtained the master degree in Chemical Engineering, in 2015 at the University of Palermo, Italy. He received the Ph.D. degree in 2019 at University of Catania. Currently, he is a Postdoctoral Researcher. His current research interests include the development of nanostructured electrochemical sensors obtained by electrochemical methods for environmental, food, pharmaceutical, biochemical and industrial control.

Maria Rita Giuffrè Research Fellow at the Fondazione Ri.MED, Palermo, Italy. Education: 2013, Bachelor's Degree in Biomedical Biotechnology, University of Palermo, Italy; 2016, Master's Degree in Medical Biotechnology, University of Milano-Bicocca, Italy; 2020, qualification to the profession of biologist, University of Salento, Italy. 2016–2017, Research Fellow at the Functional Genomics of Cancer Unit, San Raffaele Scientific Institute, Milan, Italy. 2017–2021, Research Fellow at the Department of Experimental Oncology, IEO - European Institute of Oncology, Milan, Italy. Research's topic: biological and molecular mechanisms of the immune response of the respiratory epithelium in cellular models of oxidative stress with the aim to develop an electrochemical sensor for H2O2 detection released by cells.

Elisabetta Pace fully employed Senior researcher at the National Research Council (CNR), Italy. Education, 1988: Medicine Degree at University of Palermo 1992: Diplomate of Respiratory Diseases at University of Palermo. Investigator or principal investigator in international and national competitive research projects. Principal Investigator in projects funded by Pharmaceutical Industries. Unit manager in International Clinical Trials. Component, secretary or president in examination commission for public selection. Research's topic: Lung immunopathology and pharmacology.

Chiara Cipollina is Group Leader at Fondazione Ri.MED, a research foundation based in Palermo (Italy). She obtained her PhD in Industrial Biotechnology at the University of Milano-Bicocca in 2006. As Ri.MED Fellow at the University of Pittsburgh (2008–2010), she contributed to the discovery of novel mediators of inflammation resolution. Since 2010, she works in Palermo where she studies chronic inflammation and lung disease, with a focus on cigarette smoke-associated diseases and innate immunity. Her work is unveiling a key role for inflammasome-independent activation of caspases, gasdermin cleavage and pro-inflammatory cell death in the pathogenesis of chronic lung diseases.

Alan O'Riordan received his PhD in 2005, from the University College Cork. He is a Senior Research Fellow at the Tyndall National Institute and the Principal Investigator for Smart Agri-food and Nanosensors & Systems. He coordinates/partners in a portfolio of National and EU projects and his research focuses on using nanomaterials & nanofabrication to develop end-to-end highly functional smart sensor systems, based on Raman spectroscopy and nanoelectrochemistry.

Rosalinda Inguanta is a full professor of Applied Physical Chemistry at the University of Palermo. The research concerns the synthesis of nanostructured electrochemical devices for electrochemical sensors, batteries and electrolysers, the synthesis of bio-coatings for medical devices and the recovery of precious metals from electronic waste. Currently, she coordinates/partners in a portfolio of National projects in the field of electrochemical sensors for biomedical applications and nanomaterials for energy storage and green-hydrogen production. She is involved in Technological Transfer Activity through participation in R&D projects with enterprises.